TTS in LAOS: Validation of Time Temperature Superposition under Large Amplitude Oscillatory Shear

Anja Vananroye, Pieter Leen, Peter Van Puyvelde, and Christian Clasen (✉)

Katholieke Universiteit Leuven and Leuven Materials Research Centre
Department of Chemical Engineering
W. de Croylaan 46, 3001 Leuven (Belgium)

e-mail: christian.clasen@cit.kuleuven.be
tel: ++32 16 32 23 54
fax: ++32 16 32 29 91

The validation of time-temperature superposition (TTS) of non-linear parameters obtained from large amplitude oscillatory shear (LAOS) is investigated for a model viscoelastic fluid. Oscillatory time sweeps were performed on a 11 wt% solution of high molecular weight polyisobutylene in pristane as a function of temperature and frequency and for a broad range of strain amplitudes varying from the linear to the highly non-linear regime. Lissajous curves show that this reference material displays strong non-linear behavior when the strain amplitude is exceeding a critical value. Elastic and viscous Chebyshev coefficients and alternative non-linear parameters were obtained based on the framework of Ewoldt et al. (2008) as a function of temperature, frequency, and strain amplitude. For each strain amplitude, temperature shift factors $a_T(T)$ were calculated for the first order elastic and viscous Chebyshev coefficients simultaneously, so that master curves at a certain reference temperature T_{ref} were obtained. It is shown that the expected independency of these shift factors on strain amplitude holds even in the non-linear regime. The shift factors $a_T(T)$ can be used to also superpose the higher order elastic and viscous Chebyshev coefficients and the alternative moduli and viscosities onto master curves. It was shown that the Rutgers-Delaware rule also holds for a viscoelastic solution at large strain amplitudes.

Time-temperature superposition, TTS, LAOS, Lissajous, Non-linear parameters, viscoelastic solution, Rutgers-Delaware rule

I Introduction

One of the most widely applied rheological techniques to obtain viscoelastic properties of materials consists in performing Small amplitude oscillatory shear (SAOS) tests resulting in strain amplitude (γ_0) independent storage moduli $G'(\omega)$ and loss moduli $G''(\omega)$ as a function of frequency ω (Ferry 1980; Macosko 1994). However, the independency on strain amplitude is only valid in the linear regime, where a scaled change in strain signal $\gamma(t)$ corresponds to a change in stress signal $\sigma(t)$ with the same scaling factor.

The frequency range of SAOS experiments can be extended using time-temperature superposition. For a wide class of materials such as polymer melts and solutions, changes in temperature T do not alter the shape of the linear moduli curves as a function of frequency. In a relaxation spectrum, the modulus $G(\lambda)$ of a relaxation time λ is directly proportional to the thermal energy and the number density of relaxing elements and thus to the overall fluid density ρ, so that $G \sim kT\rho$ (and this will affect all moduli equally and independent of the relaxation time). The relaxation time itself depends on the ratio of internal friction and the related internal spring constant. This spring constant for an entropic spring is directly proportional to thermal energy. For a 'thermo-rheologically simple' fluid it is assumed that the friction for each relaxation process is proportional to the same molecular friction coefficient ζ in the specific surrounding so that $\lambda \sim \zeta/kT$. Furthermore this friction coefficient ζ is also a function of the temperature T. With the assumption that all relaxation times contributing to the relaxation spectrum depend on the same internal friction coefficient ζ and thus have the same temperature dependency, a change in temperature will just shift $G'(\omega)$ and $G''(\omega)$ along the time or frequency axis. Also the similar temperature dependence of the different moduli at a given frequency shifts the whole storage or loss modulus curve along the modulus axis (Larson 1998). Applying this time-temperature superposition (TTS) principle, moduli and viscosities measured at different temperatures can be shifted horizontally and vertically with shift factors a_T and b_T respectively, to superimpose on master curves of reduced variables at an arbitrary chosen reference temperature T_{ref} (Ferry 1980):

$$G'(\omega,T) = b_T G'_r(a_T\omega, T_{ref}), \quad G''(\omega,T) = b_T G''_r(a_T\omega, T_{ref}) \qquad (1)$$

$$\eta''(\omega,T) = \frac{b_T}{a_T}\eta''_r(a_T\omega, T_{ref}), \quad \eta'(\omega,T) = \frac{b_T}{a_T}\eta'_r(a_T\omega, T_{ref}) \qquad (2)$$

The vertical shift factor b_T, introduced to account for the (small) changes in density at different temperatures, is often close to unity and can be omitted. Originally, an empirical Arrhenius type equation, with E_a the activation energy of flow and R the universal gas constant, was proposed to express the temperature dependence of the shift factor a_T:

$$a_T = \exp\left[\frac{E_a}{R}\left(\frac{1}{T} - \frac{1}{T_{ref}}\right)\right] \qquad (3)$$

This expression fits data quite good in the plateau and terminal zones for temperatures well above the glass transition temperature T_g. For polymer melts in a temperature range from T_g up to T_g+100 K, the shift factor a_T can be expressed by the Williams-Landel-Ferry (WLF) equation (Williams et al. 1955):

$$\log a_T = \frac{-c_1(T - T_{ref})}{c_2 + T - T_{ref}} \qquad (4)$$

in which c_1 and c_2 are material parameters.

The main advantage of TTS is the possibility to extend the linear viscoelastic properties to a larger time or frequency range. Examples and applications of TTS are therefore abundantly present in literature (Awasthi and Joshi 2009; Dealy and Plazek 2009; Han and Kim 1993; Oconnell and McKenna 1997; Olsen et al. 2001; Palade et al. 1995; Tajvidi et al. 2005).

Although combined SAOS/TTS measurements offer an easy tool to characterize materials within their linear regime, they often fail in describing the material properties under real processing conditions where materials are frequently subjected to large deformations and rates beyond the linear limits (Osswald 1998). In addition, a wide range of complex fluids already displays non-linear behavior

under mild processing conditions (Walker 2001; Yziquel et al. 1999). The non-linear response regime can in principle be probed by rheological tests that allow monitoring the stress response to a deformation exceeding the linear-viscoelastic limit of the fluid structure. A first category of non-linear measurements are (multi-)step shear strain experiments, where in the case of time-deformation separability, a damping function $h(\gamma)$ can be determined (Larson 1998; Rolon-Garrido and Wagner 2009). This damping function is generally experimentally obtained by vertically shifting relaxation moduli as a function of time at different strains onto a master curve. Another non-linear test method is the parallel or orthogonal superposition of a small amplitude oscillation onto a non-linear shear deformation to probe the linear response of a non-linearly deformed structure (Vermant et al. 1998; Walker et al. 2000). Parallel superposition has the disadvantage of a strong coupling between the basic shear field and the superimposed flow, which complicates the interpretation of the stress response signals (Yamamoto 1971). With orthogonal superposition the coupling is less strong, nevertheless, difficulties in instrument development limit the use (Vermant et al. 1997). A third way to characterize the non-linear viscoelastic response is by performing large amplitude oscillatory shear (LAOS) measurements with strain amplitudes *beyond* the linear limit, resulting in both frequency and strain amplitude dependent viscoelastic parameters. However, as higher order harmonics start to play a role, analyzing the response using the linear viscoelasticity theory is not valid anymore and a more sophisticated data treatment becomes necessary. Nevertheless, similar to a SAOS experiment, a LAOS experiment has the advantage of reaching a cyclic steady state which allows probing higher frequencies and faster relaxation processes than a step strain experiment. However, the transient regime before reaching a cyclic steady state in a LAOS experiment is inherently coupled with the induction of a shear history, so that the non-linear regime probed with LAOS will not be the same as with a step-strain experiment.

In the past, several methods have been proposed to analyze the non-linear data obtained from LAOS experiments. For instance, the raw stress signal $\sigma(t)$ can be graphically visualized as a function of strain $\gamma(t)$ or strain rate $\dot{\gamma}(t)$ resulting respectively in elastic or viscous Lissajous-Bowditch plots (Ewoldt et al. 2007a; Hyun et al. 2006; Philippoff 1966; Sim et al. 2003; Tee and Dealy 1975). Such curves qualitatively show evidence of non-linearities, as the shape of the closed

loops starts to deviate from an ellipsoidal shape. One of the most frequently used quantitative techniques to analyze non-linear data is Fourier-Transform (FT) rheology (Wilhelm 2002) in which the stress response signal $\sigma(t)$ is expressed as a Fourier series (Dealy and Wissbrun 1990) capturing the higher harmonics (Carotenuto et al. 2008; Fleury et al. 2004; Hyun et al. 2006; Sim et al. 2003):

$$\sigma(t) = \gamma_0 \sum_{n=odd} \left\{ G'_n(\omega, \gamma_0) \sin n\omega t + G''_n(\omega, \gamma_0) \cos n\omega t \right\} \qquad (5)$$

in which G'_n and G''_n are the elastic and viscous Fourier coefficients of order n. Recently, a generalization of linear viscoelasticity from a geometrical point of view was introduced to analyze LAOS data, based on symmetry arguments (Cho et al. 2005). This method consists of an orthogonal stress decomposition (SD) of the total stress response signal $\sigma(t)$ into an elastic contribution $\sigma'(x)$ with $x = \frac{\gamma(t)}{\gamma_0}$ and a viscous contribution $\sigma''(y)$ with $y = \frac{\dot{\gamma}(t)}{\dot{\gamma}_0}$, so that $\sigma(t) = \sigma'(t) + \sigma''(t)$. The single stress contributions $\sigma'(x)$ or $\sigma''(y)$ represent single valued functions of strain and strain rate that can be fitted by means of a polynomial regression (Cho et al. 2005). Nevertheless, for the SD analysis, the non-linear material properties represented by the polynomial coefficients were not unique since they depended on the highest order n chosen to reconstruct the signal. In addition, physical interpretation of the data based on these polynomial coefficients or on the FT coefficients is difficult. To overcome these problems, Ewoldt et al. (2008) extended the SD method of Cho et al. (2005) using a set of *orthogonal* polynomials over a finite domain. They used Chebyshev polynomials of the first kind T_n to fit the elastic stress $\sigma'(x)$ and viscous stress $\sigma''(y)$ signals:

$$\sigma'(x) = \gamma_0 \sum_{n,odd} e_n(\omega, \gamma_0) T_n(x) \qquad (6)$$

$$\sigma''(y) = \dot{\gamma}_0 \sum_{n,odd} v_n(\omega, \gamma_0) T_n(y) \qquad (7)$$

The Chebyshev polynomials $T_n(x)$ and $T_n(y)$ are symmetric, bounded and orthogonal in [-1,1]. The definition and the first few odd polynomials, used in this work, are given in Table 1.

$\boldsymbol{T_{n+1}(x)}$	=	$\boldsymbol{2xT_n(x) - T_{n-1}(x)}$
$T_0(x)$	=	1
$T_1(x)$	=	x
$T_3(x)$	=	$4x^3-3x$
$T_5(x)$	=	$16x^5-20x^3+5x$
$T_7(x)$	=	$64x^7-112x^5+56x^3-7x$

Table 1 Chebyshev polynomials of the first kind.

The elastic and viscous Chebyshev coefficients, $e_n(\omega,\gamma_0)$ and $v_n(\omega,\gamma_0)$ appearing in the stress response signals can easily be related to (or calculated from) the Fourier coefficients G'_n and G''_n obtained from FT rheology (Ewoldt et al. 2008):

$$e_n = G'_n(-1)^{(n-1)/2} \quad n = \text{odd}, \quad (8)$$

$$v_n = \frac{G''_n}{\omega} \quad n = \text{odd}. \quad (9)$$

In comparison to the polynomial coefficients of the SD analysis, the Chebyshev coefficients have the advantage that each coefficient represents a unique parameter quantifying non-linear behavior, and is independent of the other coefficients and therefore, of the order of the fit. In the linear regime, the first order coefficients recover the linear viscoelastic limits ($e_1 = G'$ and $v_1 = \eta' = G''/\omega$), whereas higher order contributions become vanishingly small. Ewoldt et al. (2008) also defined new physically meaningful elastic and viscous moduli which describe material properties at characteristic points during an oscillatory deformation cycle. The minimum strain modulus G'_M and the large strain modulus G'_L can be used to express the elastic response at an instantaneous strain of zero and at maximum strain respectively:

$$G_M^{'} \equiv \frac{d\sigma}{d\gamma}\Big|_{\gamma=0} \approx e_1 - 3e_3 + 5e_5 - 7e_7 + ... \qquad (10)$$

$$G_L^{'} \equiv \frac{\sigma}{\gamma}\Big|_{\gamma=\pm\gamma_0} \approx e_1 + e_3 + e_5 + e_7 + ... \qquad (11)$$

A graphical representation of these alternative elastic moduli is depicted in Figure 1 in the form of a Lissajous-Bowditch curve of the stress response as a function of strain. G'_L can be obtained as the slope of the secant of the elastic stress response at maximum deformation while G'_M can be found as the slope of the tangent of the elastic stress response at deformation $\gamma = 0$. Analogously, a minimum rate dynamic viscosity η'_M and a large rate dynamic viscosity η'_L express the viscous response at an instantaneous strain rate of zero and at maximum strain rate respectively.

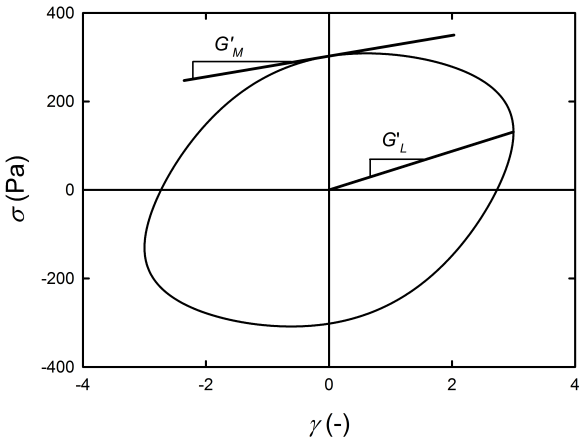

Fig. 1 Geometric interpretation of the elastic alternative moduli G'_L and G'_M obtained from a typical LAOS experiment.

On rotational devices, the combination of large deformations that are often needed to obtain non-linear behavior, and high frequencies can cause flow anomalies as a distortion of the sample free interface and finally as the loss of sample. Therefore, from an experimental point of view, the frequency regime is even more limited in the case of LAOS than in the case of linear SAOS experiments. Hence, in order to fully characterize non-linear parameters over a wide range of time scales, the applicability of the TTS principle also to the higher order harmonics is desirable. The question that arises is whether a non-linear deformation of the system is changing the internal friction coefficient ζ on which the molecular interpretation

of applicability of TTS is based. Moreover it could be questioned whether all parts of the relaxation time spectrum and the related friction coefficients are affected similarly. However, one could expect that even for such partially changed internal friction coefficients the temperature dependence is similar, and that TTS holds even in the non-linear regime. Also from constitutive models, in particular general memory integrals that include a time-deformation separability as of the Rivlin-Sawyer or K-BKZ type with factorizable kernel expressions for example of the form $G(t\text{-}t')h(\gamma)$, it is expected to have all higher order terms (which are expansions of the function $h(\gamma)$) captured by the same shift factor (Bird et al. 1987).

An experimental proof of the applicability of TTS for non-linear measurements has so far only been obtained for step strain experiments (Einaga et al. 1973; Fukuda et al. 1975; Kapnistos et al. 2009). For LAOS experiments, although they have a different non-linear deformation history than the step strain experiments, one could expect from a molecular point of view that TTS would also hold. However, there are so far no experimental reports thereon and the aim of this paper is to close this gap and to investigate the validity of TTS applied to LAOS measurements for a model viscoelastic material. The paper is structured as follows: firstly, the applicability of the TTS principle is shown for the moduli obtained in the linear viscoelastic regime of a PIB/pristane solution. Then, the non-linear behavior of this reference sample is measured over a range of frequencies and deformations and characterized in terms of Chebyshev coefficients at a reference temperature T_{ref}. Finally, it is checked whether non-linear parameters as a function of temperature can be shifted onto master curves and whether the resulting shift factors can still be fitted using the equations normally used in the linear regime.

II. Materials and methods

A. Materials

The model material chosen is a shear thinning, elastic solution of a high molecular weight polyisobutylene (PIB, Sigma-Aldrich) dissolved in 2,6,10,14-tetramethylpentadecane (pristane, Sigma-Aldrich) with a PIB mass fraction of

0.114. This fluid has similar components as the NIST Standard Reference Material SRM 2490 that shows a characteristic viscoelastic behavior similar to that of polymeric melts with the advantage of being liquid at room temperature (Schultheisz and Leigh 2002).

The two components were mixed in an amber glass bottle and time (approximately 6 months) was given for the PIB to completely dissolve while performing only a gentle agitation at room temperature to prevent degradation of the PIB (Khalil et al. 1994). The dissolution process was monitored by performing repetitive rheological measurements on the sample until no changes were observed and a stable solution was obtained. However, due to differences in PIB grade and in dissolution procedure, the absolute viscosity values and linear viscoelastic moduli differ from those of the NIST standard.

B. Methods

The *linear* viscoelastic response of the solution was determined with dynamic oscillatory measurements on a ARES strain-controlled rheometer (TA Instruments) using a 25 mm cone geometry with a cone angle of 0.04 radians and a bottom plate mounted on top of a fluid bath. The temperature was varied between 10 °C and 40 °C ± 0.1 °C. Strain sweeps were performed to determine the linear regime. For this reference material, a critical strain amplitude $\gamma_{0,crit}$ of 20 % at T = 25 °C was observed, determined as the strain amplitude at which a change of more than 3 % in moduli was seen. Subsequently, frequency sweeps with ω from 0.1 to 100 rad/s were performed at different temperatures at a strain amplitude of 6 %. Master curves for G'_r and G''_r, shown in Figure 2a, were obtained by shifting the data sets at different temperatures with respect to a reference temperature T_{ref} of 25 °C using the TTS routines of the TA Instruments Orchestrator software. For the temperature range under investigation, the data was shifted only using the horizontal shift factor a_T. We verified that it is possible to neglect the vertical shift factor b_T by plotting G''_r/G'_r as a function of $a_T\omega$ (Figure 2a), which resulted in a good master curve. For this system and at the temperatures under investigation, the temperature dependency of the shift factors $a_T(T)$, as shown in Figure 2b, could be described by the Arrhenius equation (Eq. 3) resulting in a material activation energy E_a of 30.2 kJ/mole. The Arrhenius fit resulted in slightly higher coefficients of determination R^2 compared to fits with

the WLF equation. This is expected since the measurement temperatures are strongly exceeding the glass transition temperature T_g of PIB (T_g = -70 °C) (Ferry 1980), and therefore, the Arrhenius equation will further be used to fit the $a_T(T)$ data of the following experiments.

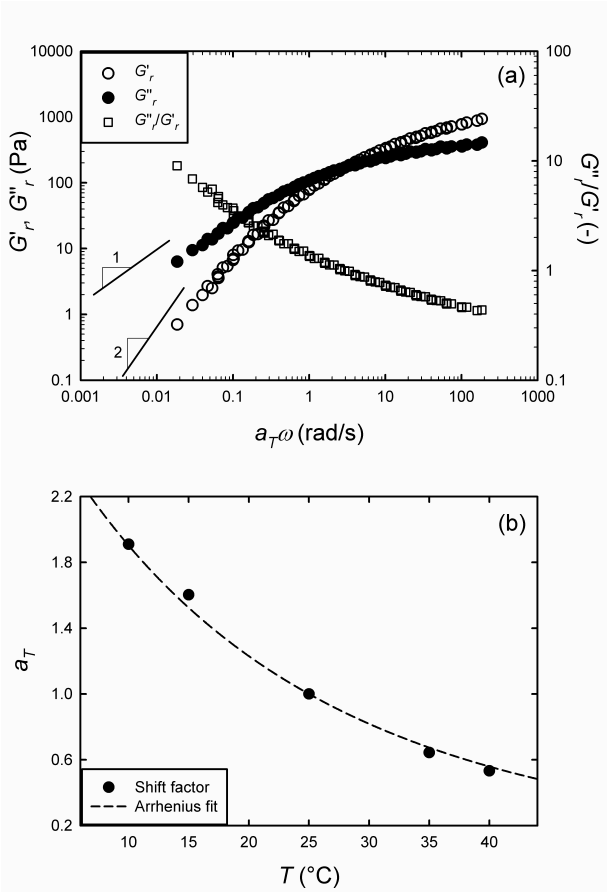

Fig. 2 (a) Linear dynamic master curves of the viscoelastic standard at T_{ref} = 25 °C. (b) Shift factor a_T and Arrhenius fit as a function of temperature T.

Non-linear LAOS measurements were obtained by performing time sweep experiments at fixed ω, γ_0, and T. Strain and torque raw data waveforms were collected using a National Instruments DAQ-Pad and TA Instruments Waveform & Fast Data Sampling software. For each set of frequency, strain amplitude and temperature, at least 10 steady-state strain and torque cycles were collected for further processing.

The freeware MATLAB-based MITlaos software package (Ewoldt et al. 2007b), was used to analyze the time-dependent strain and stress signals ($\sigma(\omega,t)$, $\gamma(\omega,t)$). The data is first trimmed to an integer number of cycles. In the present analysis, 10 entire cycles were selected for further analysis in order to reduce the effects of noise (Wilhelm et al. 1999). Secondly, a discrete Fourier transform analysis is

performed to determine the individual harmonic contributions to the system response. Based on this analysis, the order of the highest significant harmonic (defined by a ratio of harmonic amplitude to noise of greater than 1.4) was determined and the harmonics up to this order were used to reconstruct a noise-reduced stress signal for the further analysis. In the present case, the highest harmonic taken into account was of order 7. Outgoing from this reconstructed stress, the viscoelastic parameters and Chebyshev coefficients e_n and v_n are calculated and Lissajous-Bowditch curves are reconstructed.

III. Results and discussion

A. Non-linear characterization at T_{ref} = 25 °C

The non-linear oscillatory response of the reference material at a reference temperature T_{ref} of 25 °C is shown in the form of Pipkin diagrams (Pipkin 1972). In Figure 3 the effect of strain and frequency on the mechanical behavior of a material is visualized by means of normalized Lissajous-Bowditch curves. The Lissajous-Bowditch curves in Figure 3a give for each combination of frequency ω and strain amplitude γ_0 the total stress response $\sigma(t)$ as a function of strain $\gamma(t)$ (full closed loops), and the elastic component $\sigma'(x)$ (dotted line) from the orthogonal stress decomposition (Eq. 6). Both stress signals are normalized by the maximum stress amplitude σ_{max} of which the values are indicated on each Lissajous-Bowditch plot. Similarly, Figure 3b shows the viscous response by plotting the normalized total stress response $\sigma(t)/\sigma_{\max}$ as a function of the strain rate $\dot{\gamma}(t)$ (full closed loops), and the normalized purely viscous component $\sigma''(y)/\sigma_{\max}$ (dotted line) from the orthogonal stress decomposition (Eq. 7). The total stresses $\sigma(t)$ in Figure 3 are reconstructed from the measured Fourier coefficients G'_n and G''_n up to a highest harmonic $n_{max} = 7$ to remove noise from the data (Fourier coefficients for harmonics higher than $n = 7$ are negligible in the present case even for the highest amplitude and frequency). The higher harmonics determined for each measurement in Figure 3 are compiled in form of the elastic and viscous Chebyshev coefficients e_n and v_n as a function of frequency (for a compilation of all Chebyshev coefficients see Figure 11 in the Appendix that

contains also the data from different temperatures shifted with TTS as shown in the following section).

At a strain amplitude of 6 %, the Lissajous-Bowditch curves can be approximated by ellipses, indicating that the material displays linear viscoelastic behavior. In these cases, the elastic and viscous contributions (dotted lines) are straight lines. The large strain modulus G'_L and minimum strain modulus G'_M reduce to e_1 (or the linear storage modulus G') and the alternative dynamic viscosities η'_L and η'_M are equal to $G''\omega = \eta'$. Note that at the lowest frequencies shown for the strain amplitude of 6 %, some overfitting of the stress response is seen due to the high ratio of noise compared to the G'_n and G''_n at the higher harmonics (for consistency, all harmonics up to $n = 7$ are used in Figure 3 to construct the strain curves even at the lowest strain amplitude).

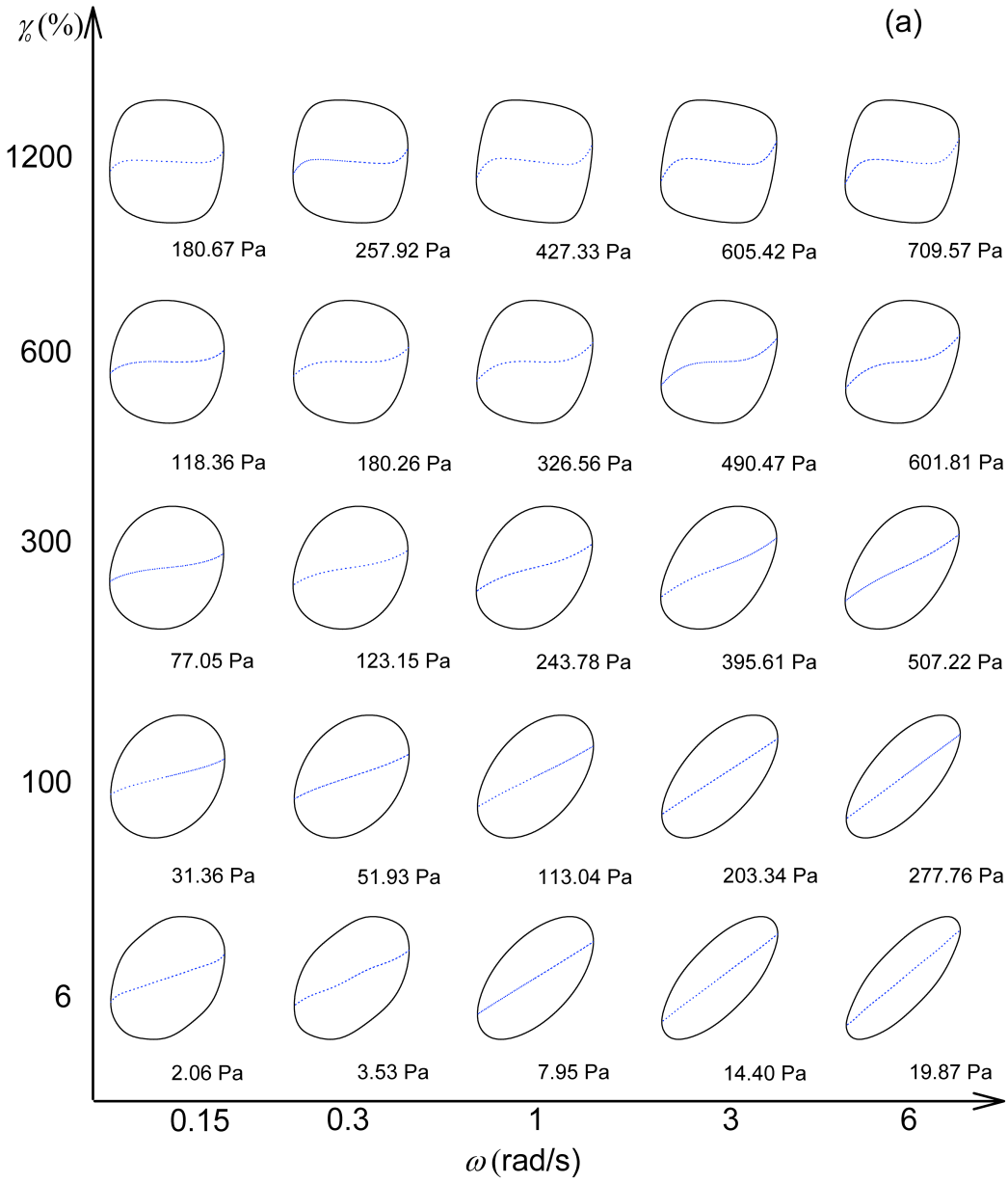
γ(%)
(a)
1200
600
300
100
6
180.67 Pa
257.92 Pa
427.33 Pa
605.42 Pa
709.57 Pa
118.36 Pa
180.26 Pa
326.56 Pa
490.47 Pa
601.81 Pa
77.05 Pa
123.15 Pa
243.78 Pa
395.61 Pa
507.22 Pa
31.36 Pa
51.93 Pa
113.04 Pa
203.34 Pa
277.76 Pa
2.06 Pa
3.53 Pa
7.95 Pa
14.40 Pa
19.87 Pa
0.15
0.3
1
3
6
ω(rad/s)

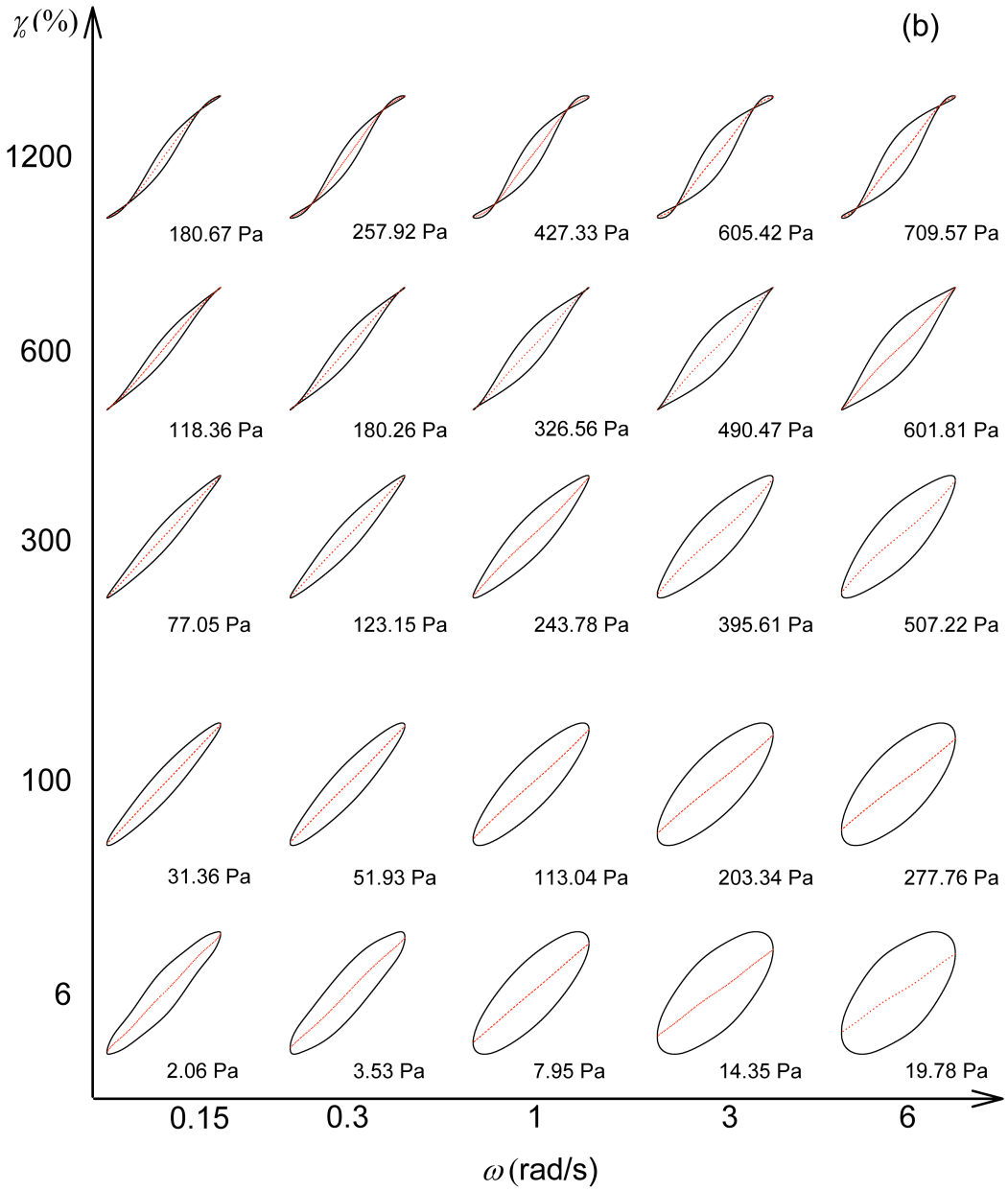

Fig. 3 Normalized Lissajous-Bowditch curves at T = 25 °C. (a) Normalized total stress response $\sigma(t)/\sigma_{max}$ (full line) and elastic stress response $\sigma'(t)/\sigma_{max}$ (dotted line) as a function of normalized strain $\gamma(t)/\gamma_0$ and (b) normalized total stress response $\sigma(t)/\sigma_{max}$ (full line) and viscous stress response $\sigma''(t)/\sigma_{max}$ (dotted line) as a function of normalized strain rate $\dot{\gamma}(t)/\dot{\gamma}_0$. The maximum stresses σ_{max} are added for each combination of frequency and strain amplitude.

With increasing strain amplitude γ_0, the total response starts to deviate from an ellipsoidal shape as non-linearities are evolving. In these cases, the elastic and viscous contributions are not represented by straight lines anymore and hence, a single elastic or viscous modulus is insufficient to describe the local elastic or viscous behavior. In Figure 3a for instance, it is seen at high strain amplitudes (γ_0

= 600 %, γ_0 = 1200 %) that G'_L (slope of the secant of the elastic stress response at maximum deformation) is high compared to G'_M (slope of the tangent of the elastic stress response at deformation γ_0 = 0), indicating that the PIB in pristane reference material behaves strain stiffening at high strain amplitudes. Figure 4 shows the first order Chebyshev coefficients e_1 (= G'_1) and the local elastic moduli G'_M and G'_L at a selected frequency of ω = 1 rad/s as a function of the imposed strain amplitude γ_0. At low strain amplitudes (γ_0 = 6 %) all three elastic moduli converge to the linear storage modulus G', indicating that linear behavior prevails. With increasing strain amplitude, though all moduli simultaneously decrease, a clear divergence between the moduli is developing. The large strain modulus G'_L decreases less than the minimum strain modulus G'_M indicating that the elastic response behaves strain stiffening at high strain amplitudes. e_1 is a weighted average of the elastic response in a strain cycle with $e_1 \cong$ ¼ ($3G'_L$ + G'_M). At strain amplitudes of 600 % and beyond the minimum strain modulus G'_M becomes even negative (dotted line at y = 0 in Figure 3a), indicating that the material is instantaneously releasing more elastic stress than it is accumulating by the deformation (Ewoldt et al. 2008). This relates to secondary loops in the total response signal as a function of strain rate (Figure 3b), a phenomenon explained by Ewoldt and McKinley (2010) and corresponds to the stress overshoot in steady shear startup experiments on polymer solutions, which is attributed to shear-enhanced disentanglements. The most important distinction is that the LAOS flow field is periodically reversed, and that the changes in microstructure must reform under the timescales of the oscillation to reversibly achieve negative G'_M values.

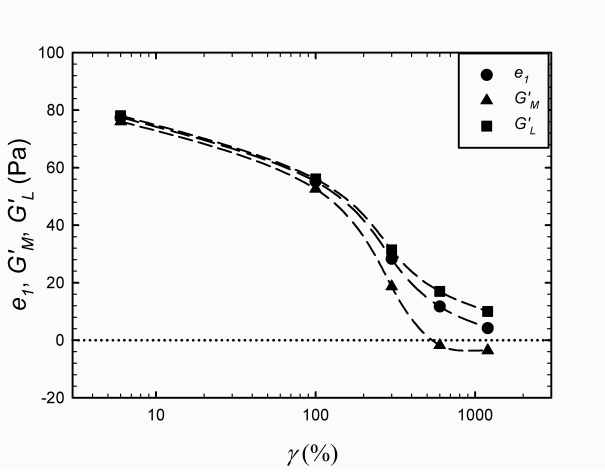

Fig. 4 Elastic moduli G'_L, G'_M, and e_1 as a function of strain amplitude γ_0 for ω = 1 rad/s and T = 25 °C. Lines are added to guide the eye.

Figure 5 shows the evolution of the elastic large strain modulus G'_L (Figure 5a) and the elastic minimum strain modulus G'_M (Figure 5b) as a function of frequency ω and strain amplitude γ_0 at T = 25 °C. For all strain amplitudes applied, G'_L increases with increasing frequency, similar as in the linear regime. For G'_M, this similarity only holds for strain amplitudes up to 300 %. The minimum strain modulus at high strain amplitudes shows specific behavior as can be seen on the inset of Figure 5b (linear-log scale). At a strain amplitude of 600 %, first a decrease of G'_M with frequency is observed followed by an increase for $\omega > 1$ rad/s, whereas for a strain amplitude of 1200 %, a decreasing trend is seen up to $\omega = 6$ rad/s. Furthermore, the decreasing G'_M eventually becomes negative.

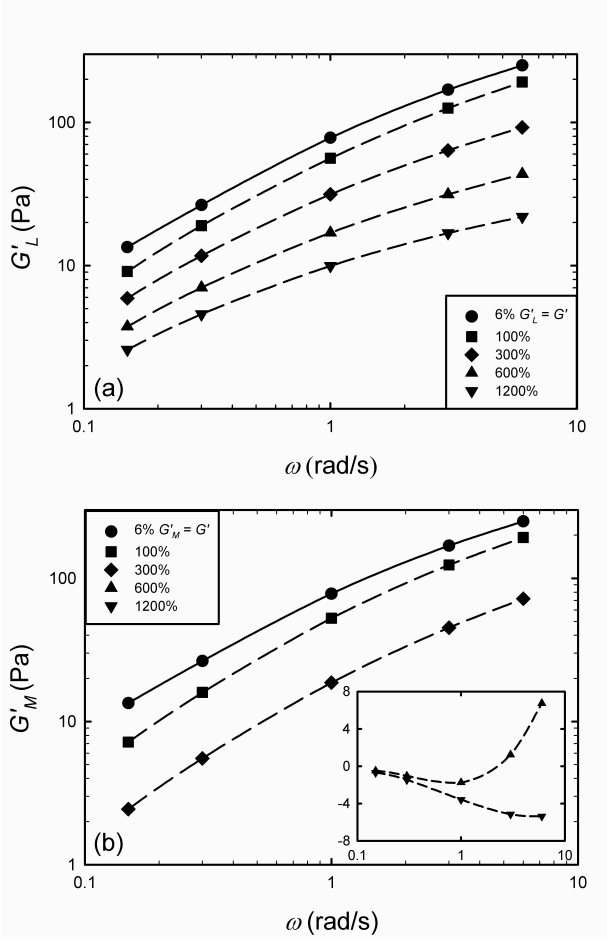

Fig. 5 Evolution of (a) the large strain modulus G'_L and (b) the minimum strain modulus G'_M as a function of strain amplitude γ_0 and frequency ω at T = 25 °C. Lines are added to guide the eye.

B. TTS shift for Chebyshev coefficients e_n and v_n

In the second part, the temperature dependent shift factors for the first order Chebyshev coefficients e_1 and v_1 were determined for all strain amplitudes. Figure 6 shows an example of the effect of temperature on the elastic (Figure 6a) and viscous (Figure 6b) first order Chebyshev coefficients e_1 and v_1 at a strain amplitude γ_0 of 1200 %.

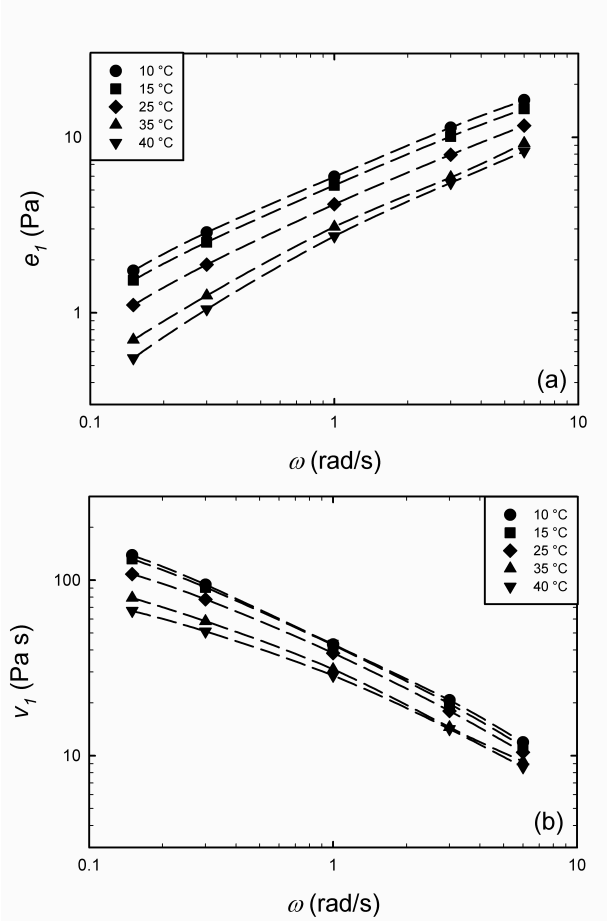

Fig. 6 Temperature dependence of (a) the elastic Chebyshev coefficients e_1 and (b) the viscous Chebyshev coefficients v_1 at a strain amplitude γ_0 of 1200 % as a function of frequency ω. Lines are added to guide the eye.

All curves in Figure 6 display the same trend as a function of frequency, irrespective of the temperature, and similar results were also seen at other strain amplitudes, indicating that master curves using shift factors could be obtained. For each strain amplitude, the shift factors $a_T(T)$ were calculated with respect to a reference temperature T_{ref} of 25 °C based on a residual minimization algorithm for a joint shifting of the first order viscous and elastic Chebyshev coefficients. For all investigated strain amplitudes from 6 to 1200 %, e_1 and v_1 coefficients could

be simultaneously shifted for each strain amplitude, resulting in horizontal shift factors $a_T(T)$ independent of the elastic or viscous character of the Chebyshev coefficients. Again, it was verified that vertical shift factor b_T could be omitted. This resulted in an $e_{1,r}$ versus $a_T\omega$ master curve (as shown for example for γ_0 = 1200 % by the filled diamonds in Figure 7) and a $v_{1,r}/a_T$ versus $a_T\omega$ master curve. The obtained shift factors $a_T(T)$ for e_1 and v_1 at each strain amplitude could also be used to superpose all other e_n and v_n coefficients up to n = 7. An example of the resulting master curves at T_{ref} = 25 °C for the reduced elastic Chebyshev coefficients $e_{n,r}$ is shown in Figure 7 for a strain amplitude of 1200 %. A complete overview of all master curves for both the elastic Chebyshev coefficients $e_{n,r}$ and viscous Chebyshev coefficients $v_{n,r}/a_T$ for strain amplitudes from 100 to 1200 % is shown in Figure 11 in the Appendix. For a strain amplitude of 6 % which is in the linear regime, all higher order Chebyshev coefficients were negligible, as expected. For strain amplitudes of 100 and 300 %, elastic and viscous contributions up to the third order and for a strain amplitude of 600 % Chebyshev coefficients up to the fifth order could be measured and were taken into account for superposition. A general lower limit for the determination of all Chebyshev coefficients with the current setup was determined to be of O(0.01 Pa). Since results are presented on a logarithmic scale in Figures 7 and 11, absolute values of the coefficients are shown and negative values are indicated as open symbols.

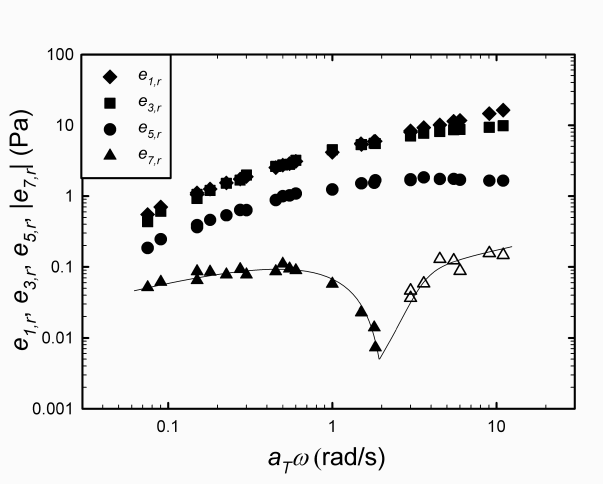

Fig. 7 Master curves at T_{ref} = 25 °C for the absolute values of the reduced elastic Chebyshev coefficients $e_{n,r}$ at a strain amplitude γ_0 of 1200 % as a function of reduced frequency $a_T\omega$. Filled symbols represent positive values, open symbols represent negative values. The line is added to guide the eye.

The fact that the same values of a_T superpose all the viscoelastic functions is one of the criteria for applicability of the TTS procedure (Ferry 1980) to non-linear data also for LAOS experiments. In Figure 8, the obtained shift factors a_T are plotted as a function of temperature for each of the strain amplitudes under investigation. As can be seen, results indicate that the shift factors are mainly independent of strain amplitude in the non-linear regime, at least in the strain amplitude range explored here.

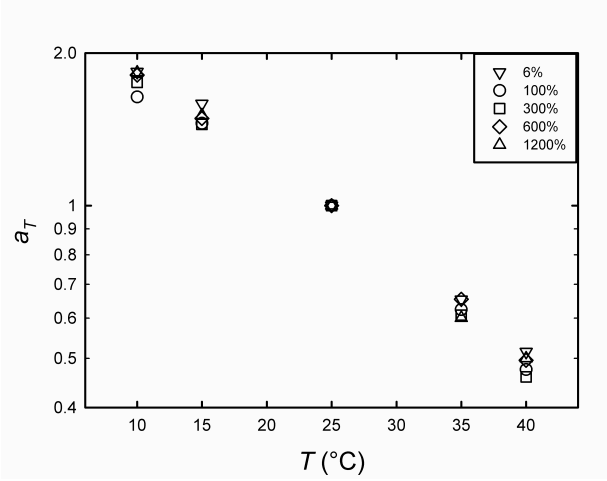

Fig. 8 Shift factors a_T as a function of temperature and strain amplitude for T_{ref} = 25 °C.

Next, it was checked whether the $a_T(T)$ curves could still be fitted using the Arrhenius equation as expressed in Eq. 3. Results for the Arrhenius fit parameters E_a are summarized in Table 2 as a function of strain amplitude together with the coefficients of determination R^2.

Strain amplitude (%)	**6**	**100**	**300**	**600**	**1200**
E_a **(kJ/mol)** R^2	29.8 0.992	25.4 0.966	27.5 0.977	28.5 0.993	29.3 0.990

Table 2 Fit parameters E_a and coefficients of determination R^2 obtained by fitting the shift factors $a_T(T)$ of the first order Chebyshev coefficients e_1 and v_1 using Eq. 3.

As a function of strain amplitude in the non-linear regime, activation energy values slightly increase from 25.4 to 29.3 kJ/mole, though the differences in E_a still remain small. Hence, one could say that all Chebyshev coefficients can still be reasonably shifted using the same a_T factors independent of the applied strain amplitude. The coefficients of determination R^2 in the fit approach were all above 0.96 and the fit parameter E_a can still be referred to as the activation energy of

flow of the system under investigation, since values in the linear and non-linear regime are quite similar. Based on the combined shifting of e_1 and v_1, an average value for the activation energy E_a of 28.1 kJ/mole can be assumed. The remark has to be made that this average value is slightly below the value of 30.2 kJ/mole, obtained after simultaneously rescaling G' and G'' from the frequency sweep data in the linear regime (Figure 2).

A closer look at the reduced Chebyshev coefficients in Figure 11 shows that increasing the strain amplitude generally has a stronger effect on the magnitude of the elastic coefficients $e_{n,r}$ than on the viscous coefficients $v_{n,r}$ for the investigated system. In particular the first order elastic coefficient $e_{1,r}$ shows a much stronger decrease with strain amplitude than the viscous coefficient $v_{1,r}$. This domination of the viscous contribution to the non-linear response of the sample at high deformations can also be seen when comparing the dissipated energy in the LAOS experiments to the viscosity of a steady state shear rate experiment. In analogy to the Rutgers-Delaware rule (Doraiswamy et al. 1991). Figure 9 shows $v_{1,r}/a_T$, which gives the total dissipated energy (Ewoldt et al. 2008; Ganeriwala and Rotz 1987; Giacomin and Oakley 1992) as a function of the reduced shear rate amplitude $a_T\omega\gamma_0$ at T_{ref} = 25 °C. The Rutgers-Delaware rule was originally developed for yield stress fluids that exhibit an inelastic, shear thinning behavior in an oscillatory shear experiment once the yield stress is overcome. For yield stress fluids, the rule holds only for strain amplitudes that are so large that the shear stresses created in the yielded state are large in comparison to the elastic stresses that are stored in the unyielded state of a deformation cycle. Similarly, the Rutgers-Delaware rule holds for a viscoelastic solution only when the magnitude of viscous Chebyshev coefficients is large in comparison to the elastic coefficients. As it can be seen in Figure 9, a strain amplitude of 100 % does not lead to an overlap of $v_{1,r}/a_T$ with the steady shear viscosity at T_{ref} = 25°C. A comparison of the non-linear viscous moduli $v_{n,r}\omega$ with the respective $e_{n,r}$ from Figure 11 for a strain amplitude of 100 % shows that both still have a similar order of magnitude. Only when applying higher strain amplitudes of 300 % and larger, the viscous modulus $v_{1,r}\omega$ starts to dominate and the dynamic values in Figure 9 start to superpose onto the steady shear data. The sample responds to large deformation in LAOS mainly in a shear thinning manner. This observation can also be related to the observed elastic response to high shear rates at large

deformations. As shown in Figures 5 and 12, the minimum strain modulus G'M (eq. 10) (that gives an elastic modulus at an instantaneous strain of zero, and therefore at the maximum strain rate) becomes small with increasing strain amplitude and eventually, becomes negative. At the maximum strain rate when subjected to large deformations during a deformation cycle, the entangled polymer solution is releasing more elastic stress then it is accumulating.

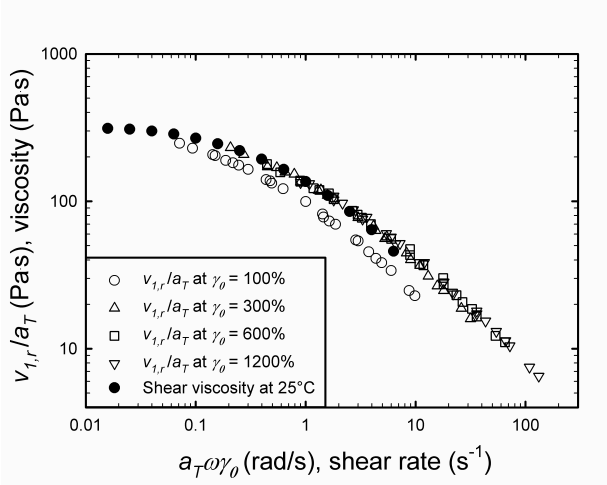

Fig. 9 Comparison of reduced first order Chebychev coefficients $v_{1,r}/a_T$ as a function of reduced shear rate amplitude $a_T\omega\gamma_0$ with steady state shear viscosity data as a function of shear rate at T_{ref} = 25 °C.

C. TTS shift for alternative elastic moduli and dynamic viscosities

Since all Chebyshev coefficients up to order n = 7 could be shifted using the same $a_T(T)$, it is expected based on the definitions of the alternative non-linear moduli and viscosities in Eqs. 10 and 11, that also the elastic moduli G'_L and G'_M and the alternative dynamic viscosities η'_L and η'_M can be shifted onto master curves. In Figure 10, an example of such TTS master curves at a strain amplitude of 1200 % is shown for the reduced large strain modulus $G'_{L,r}$ and for the reduced minimum strain modulus $G'_{M,r}$ as a function of reduced frequency $a_T\omega$ (using the shift factors $a_T(T)$ obtained for the first order Chebyshev coefficients at the appropriate strain amplitude (Figure 8)). Results at other strain amplitudes for the reduced alternative elastic moduli and for the reduced alternative dynamic moduli are given in Figure 12 in the Appendix. In general, for all applied strain amplitudes, G'_L, η'_L and η'_M data could be shifted onto master curves simply using the shift factors $a_T(T)$ from Fig. 8. One thing to recognize for $G'_{M,r}$ in Figure 10 for a strain

amplitude of 1200 % (and also in Figure 12 for a strain amplitude of 600 %), is that shifting the absolute values for $G'_{M,r}$ results in an apparently higher degree of scatter on the master curves of more than an order of magnitude above the lower determination limit of O(0.01 Pa) for the Chebyshev coefficients. The scatter on the $G'_{M,r}$ data results from two issues: the contribution of higher order harmonics to $G'_{M,r}$ is amplified since the higher order $e_{n,r}$ enter multiplied with their order number n. Hence, the relatively small degree of scatter seen for the higher order harmonics $e_{n,r}$ (see Figure 11 in the Appendix) contributes to a larger degree to the scatter at high strain amplitudes for the $G'_{M,r}$ data. Furthermore, the third order term enters Eq. 10 as a negative value, which, for example for the case of 600 % strain amplitude in Figure 11 cancels the contribution from $e_{1,r}$ and leaves $e_{5,r}$ (that was determined at the lower resolution limit) as the dominant contribution.

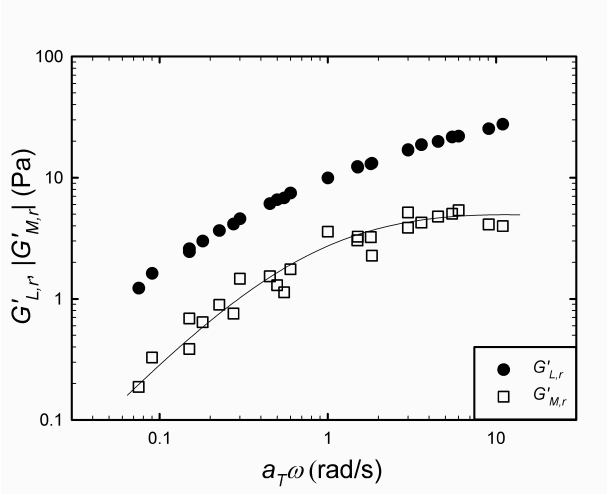

Fig. 10 Master curves at T_{ref} = 25 °C for the reduced large strain modulus $G'_{L,r}$ and for the absolute values of the reduced minimum strain modulus $G'_{M,r}$ at a strain amplitude γ_0 of 1200 % as a function of reduced frequency $a_T\omega$. Filled symbols represent positive values, open symbols represent negative values. The line is added to guide the eye.

IV. Conclusions

The expected applicability of TTS also to non-linear LAOS measurements could be experimentally verified for a thermo-rheologically simple fluid. This offers the possibility to construct master curves over an extended range of frequencies and strain amplitudes and to counteract the inherently reduced frequency range for a single LAOS experiments due to the occurrence of flow anomalies at higher deformation rates in the non-linear regime. Such master curves could be used to

characterize materials that show non-linear behavior under typical processing conditions which can be highly useful for processing industries. It was shown that horizontal shift factors $a_T(T)$ obtained for the first order Chebyshev coefficients can also be used to shift the higher order Chebyshev coefficients as well as other non-linear parameters at the same strain amplitude. In addition, it was seen that these shift factors $a_T(T)$ are independent of strain amplitude, and hence also valid in the non-linear response regime. Nevertheless, when performing TTS, whether it is in the linear or non-linear regime, one must be aware that shift factors valid in specific regions of frequency and strain amplitude, might not apply to others and the data analysis always has to be carefully monitored (Dealy and Plazek 2009). For the investigated model polymer solution it could be shown that the Rutgers-Delaware rule also holds for a viscoelastic solution if the deformation is high enough. This superposition of the first order viscous Chebyshev coefficient v_1 as a function of the shear rate amplitude $\gamma_0\omega$ onto the steady state flow curve only holds if the magnitude of the non-linear elastic moduli becomes small compared to the viscous coefficients.

Acknowledgments

The authors acknowledge the Research Foundation - Flanders (FWO Vlaanderen - post doctoral fellowship of A. Vananroye) and Onderzoeksfonds K.U.Leuven (GOA 03/06) for financial support. CC would like to acknowledge financial support from the ERC starting grant no. 203043 – NANOFIB. Dr Ewoldt is gratefully acknowledged for providing the MITlaos software.

References

Awasthi V, Joshi YM (2009) Effect of temperature on aging and time-temperature superposition in nonergodic laponite suspensions. Soft Matter 5 (24):4991-4996. doi:10.1039/b915105b

Bird RB, Armstrong RC, Hassager O (1987) Dynamics of polymer liquids, vol 1: Fluid mechanics. second edn. Wiley, New York

Carotenuto C, Grosso M, Maffettone PL (2008) Fourier transform rheology of dilute immiscible polymer blends: A novel procedure to probe blend morphology. Macromolecules 41 (12):4492-4500. doi:10.1021/ma800540n

Cho KS, Hyun K, Ahn KH, Lee SJ (2005) A geometrical interpretation of large amplitude oscillatory shear response. Journal of Rheology 49 (3):747-758. doi:10.1122/1.1895801

Dealy JM, Plazek D (2009) Time temperature superposition - a users guide. Rheology Bulletin 78 (2):16-31

Dealy JM, Wissbrun KF (1990) Melt Rheology and Its Role in Plastics Processing: Theory and Applications. Van Nostrand Reinhold, New York

Doraiswamy D, Mujumdar AN, Tsao I, Beris AN, Danforth SC, Metzner AB (1991) The Cox-Merz rule extended - a rheological model for concentrated suspensions and other materials with a yield stress. Journal of Rheology 35 (4):647-685

Einaga Y, Osaki K, Kimura S, Yamada N, Tamura M, Kurata M (1973) Stress relaxation of polymer-solutions under large strain. Polymer Journal 5 (1):91-96

Ewoldt RH, Clasen C, Hosoi AE, McKinley GH (2007a) Rheological fingerprinting of gastropod pedal mucus and synthetic complex fluids for biomimicking adhesive locomotion. Soft Matter 3 (5):634-643. doi:10.1039/b615546d

Ewoldt RH, Hosoi AE, McKinley GH (2008) New measures for characterizing nonlinear viscoelasticity in large amplitude oscillatory shear. Journal of Rheology 52 (6):1427-1458. doi:10.1122/1.2970095

Ewoldt RH, McKinley GH (2010) On secondary loops in LAOS via self-intersection of Lissajous-Bowditch curves. Rheologica Acta 49 (2):213-219. doi:10.1007/s00397-009-0408-2

Ewoldt RH, Winter PB, G.H. M (2007b) MITlaos user manual version 2.1 Beta for MATLAB. MITlaos@mitedu

Ferry JD (1980) Viscoelastic properties of polymers (3rd edition). Wiley, New York

Fleury G, Schlatter G, Muller R (2004) Non linear rheology for long chain branching characterization, comparison of two methodologies: Fourier transform rheology and relaxation. Rheologica Acta 44 (2):174-187. doi:10.1007/s00397-004-0394-3

Fukuda M, Osaki K, Kurata M (1975) Nonlinear viscoelasticity of polystyrene solutions.1. Strain-dependent relaxation modulus. Journal of Polymer Science Part B-Polymer Physics 13 (8):1563-1576

Ganeriwala SN, Rotz CA (1987) Fourier-transform mechanical analysis for determining the nonlinear viscoelastic properties of polymers. Polymer Engineering and Science 27 (2):165-178

Giacomin AJ, Oakley JG (1992) Structural network models for molten plastics evaluated in large-amplitude oscillatory shear Journal of Rheology 36 (8):1529-1546

Han CD, Kim JK (1993) On the use of time-temperature superposition in multicomponent multiphase polymer systems. Polymer 34 (12):2533-2539

Hyun K, Nam JG, Wilhelm M, Ahn KH, Lee SJ (2006) Large amplitude oscillatory shear behavior of PEO-PPO-PEO triblock copolymer solutions. Rheologica Acta 45 (3):239-249. doi:10.1007/s00397-005-0014-x

Kapnistos M, Kirkwood KM, Ramirez J, Vlassopoulos D, Leal LG (2009) Nonlinear rheology of model comb polymers. Journal of rheology 53 (5):1133-1153. doi:10.1122/1.3191781

Khalil K, Tougui A, Sigli D (1994) Relation between some rheological properties of polyisobutylene solutions and their mode of proparation. Journal of Non-Newtonian Fluid Mechanics 52 (3):375-386

Larson RG (1998) The Structure and Rheology of Complex Fluids. Oxford University Press, New York

Macosko CW (1994) Rheology: principles, measurements, and applications. Wiley-VCH, New York

Oconnell PA, McKenna GB (1997) Large deformation response of polycarbonate: Time-temperature, time-aging time, and time-strain superposition. Polymer Engineering and Science 37 (9):1485-1495

Olsen NB, Christensen T, Dyre JC (2001) Time-temperature superposition in viscous liquids. Physical Review Letters 86 (7):1271-1274

Osswald TA (1998) Polymer processing fundamentals. Carl Hanser Verlag, Munich

Palade LI, Verney V, Attane P (1995) Time-temperature superposition and linear viscoelasticity of polybutadienes. Macromolecules 28 (21):7051-7057

Philippoff W (1966) Vibrational measurements with large amplitudes. Transactions of the Society of Rheology 10 (1):317-334

Pipkin AC (1972) Lectures on viscoelasticity theory. Springer, New York

Rolon-Garrido VH, Wagner MH (2009) The damping function in rheology. Rheologica Acta 48 (3):245-284. doi:10.1007/s00397-008-0308-x

Schultheisz CR, Leigh SJ (2002) Certification of the rheological behavior of SRM 2490, polyisobutylene dissolved in 2,6,10,14-tetramethylpentadecane. National Institute of Standards and technology special publication 262-143, Gaithersburg

Sim HG, Ahn KH, Lee SJ (2003) Large amplitude oscillatory shear behavior of complex fluids investigated by a network model: a guideline for classification. Journal of Non-Newtonian Fluid Mechanics 112 (2-3):237-250. doi:10.1016/s0377-0257(03)00102-2

Tajvidi M, Falk RH, Hermanson JC (2005) Time-temperature superposition principle applied to a kenaf-fiber/high-density polyethylene composite. Journal of Applied Polymer Science 97 (5):1995-2004. doi:10.1002/app.21648

Tee TT, Dealy JM (1975) Nonlinear viscoelasticity of polymer melts. Transactions of the Society of Rheology 19 (4):595-615

Vermant J, Moldenaers P, Mewis J, Ellis M, Garritano R (1997) Orthogonal superposition measurements using a rheometer equipped with a force rebalanced transducer. Review of Scientific Instruments 68 (11):4090-4096

Vermant J, Walker L, Moldenaers P, Mewis J (1998) Orthogonal versus parallel superposition measurements. Journal of Non-Newtonian Fluid Mechanics 79 (2-3):173-189

Walker LM (2001) Rheology and structure of worm-like micelles. Current Opinion in Colloid & Interface Science 6 (5-6):451-456

Walker LM, Vermant J, Moldenaers P, Mewis J (2000) Orthogonal and parallel superposition measurements on lyotropic liquid crystalline polymers. Rheologica Acta 39 (1):26-37

Wilhelm M (2002) Fourier-Transform rheology. Macromolecular Materials and Engineering 287 (2):83-105

Wilhelm M, Reinheimer P, Ortseifer M (1999) High sensitivity Fourier-transform rheology. Rheologica Acta 38 (4):349-356

Williams ML, Landel RF, Ferry JD (1955) The temperature dependence of relaxation mechanisms in amorphous polymers and other glass-forming liquids Journal of the American Chemical Society 77 (14):3701-3707

Yamamoto M (1971) Rate-dependent relaxation spectra and their determination. Transactions of the Society of Rheology 15:331-344

Yziquel F, Carreau PJ, Tanguy PA (1999) Non-linear viscoelastic behavior of fumed silica suspensions. Rheologica Acta 38 (1):14-25

APPENDIX

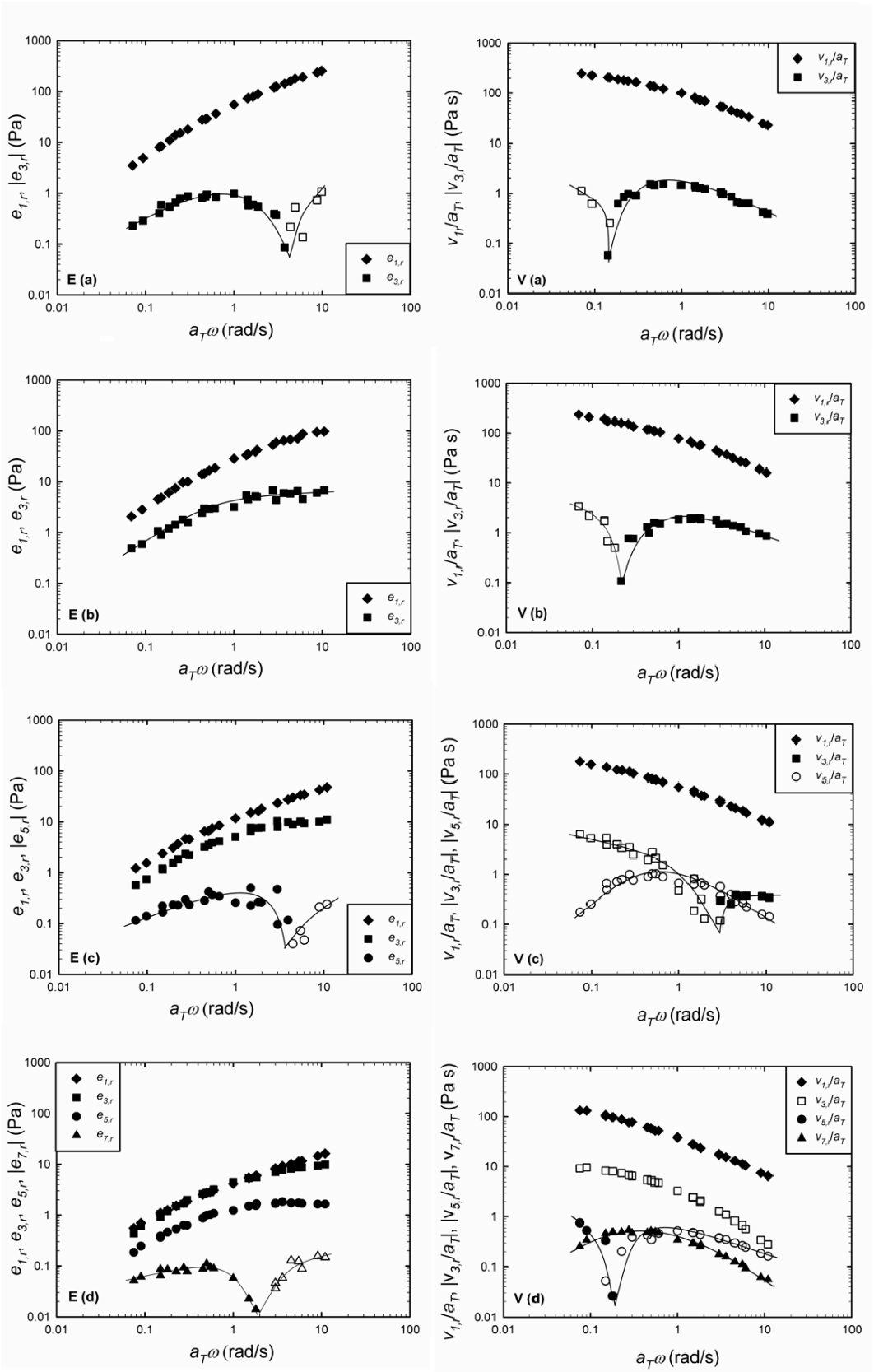

Fig. 11 Master curves after performing TTS shift for (E) the reduced elastic and (V) reduced viscous Chebyshev coefficients at a strain amplitude of (a) 100 %, (b) 300 %, (c) 600 %, and (d) 1200 %. Open symbols represent negative values. Lines are added to guide the eye.

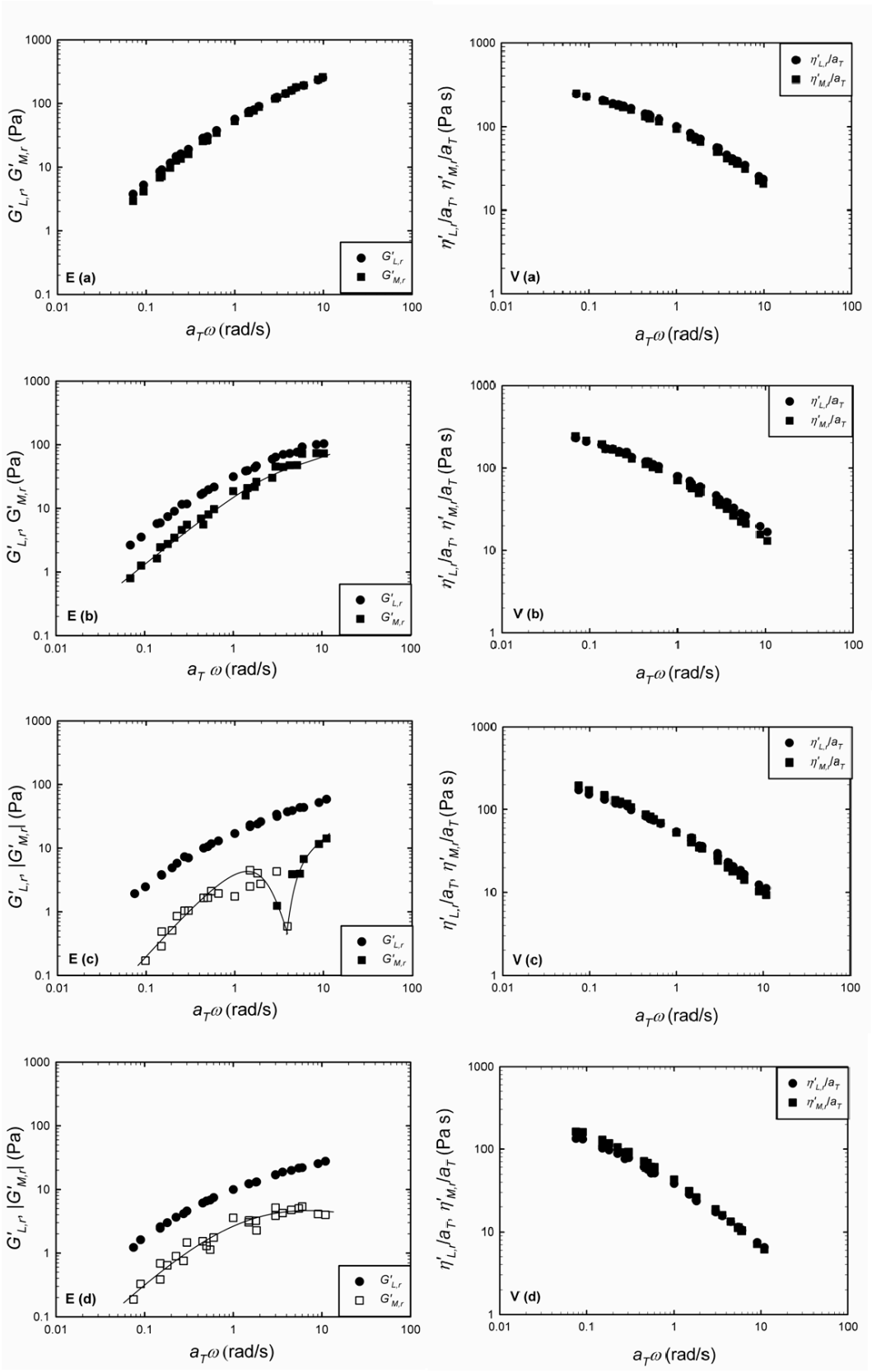

Fig. 12 Master curves after performing TTS shift for (E) the reduced elastic moduli and (V) reduced dynamic viscosities at a strain amplitude of (a) 100 %, (b) 300 %, (c) 600 %, and (d) 1200 %. Open symbols represent negative values. Lines are added to guide the eye.